Processing and Application of Ceramics 10 [4] (2016) 201–208
DOI: 10.2298/PAC1604201C

Comprehensive characterization of $BiFeO_3$ powder synthesized by the hydrothermal procedure

Maria Čebela[1,*], Bojan Janković[2], Radmila Hercigonja[2], Miodrag J. Lukić[3], Zorana Dohčević-Mitrović[4], Dušan Milivojević[5], Branko Matović[1]

[1]*Laboratory of Materials Science, University of Belgrade, "Vinča" Institute of Nuclear Sciences, Belgrade, Serbia*
[2]*Faculty of Physical Chemistry, University of Belgrade, Studentski trg 12-16, P. O. Box 137, 11001 Belgrade, Serbia*
[3]*Institute of Technical Sciences of the Serbian Academy of Sciences and Arts, Knez Mihailova 35/IV, Belgrade 11000, Serbia*
[4]*Center for Solid State Physics and New Materials, Institute of Physics, University of Belgrade, Pregrevica 118, 11080 Belgrade, Serbia*
[5]*Department of Radiation Chemistry and Physics, University of Belgrade, "Vinča" Institute of Nuclear Sciences, Belgrade, Serbia*

Received 24 June 2016; Received in revised form 7 October 2016; Accepted 30 October 2016

Abstract

In this paper, bismuth ferrite (BFO) particles synthesized by controlled hydrothermal process, where the particles of small sizes and with high purity were obtained. Structural analysis showed that non-annealed powder can be perfectly fitted to rhombohedral space group R3c and contains a very small amount of secondary phase, whereas the final product (annealed at 800 °C) represents single-phase perovskite powder with high crystallinity. HRTEM analysis confirmed existence of twin stacking faults, which are responsible for enhanced magnetic properties. EPR measurements suggested existence of electrons trapped by vacancies or defects. It has been proposed that existence of $Fe^{3+}-O_V$ defect complex could be generated at elevated temperatures followed by formation of trivalent Fe ions, which intensely provide local 3d moments.

Keywords: *multiferroics, $BiFeO_3$, microstructure, electronic paramagnetic resonance, magnetic properties*

I. Introduction

Lately, there has been an increasing interest for materials which simultaneously respond to the various external influences, such as thermal, electrical, magnetic and mechanical factors. Because of their multi-functionality, the constituent elements react to different combinations of external influences. The multi-function elements can be easily combined into a so-called "smart systems", which represent a combination of different sensors, actuators and electronics. For a long time, the most usable materials for the electromechanical applications, such as sensors and actuators, based on lead perovskites, including the most common $Pb(Zr,Ti)O_3$ (PZT), are attracting the most attention. Despite the excellent functional characteristics and exceptional flexibility for different applications, these materials are harmful to humans and the environment due to the high levels of lead. The intensive search for the material with similar electromechanical properties which is lead-free represents the primary goal in the field of piezoelectric ceramic materials. Despite the progress in application of materials without lead (although in a very narrow range of application), there remains a need to discover a material which would be a complete replacement for PZT. The solution of this problem should be a subject for future research [1].

Bismuth ferrite ($BiFeO_3$) has recently drawn atten-

*Corresponding author: tel: +381 11 3408 744,
fax: +381 11 3408 224, e-mail: *mcebela@vinca.rs*

tion due to its outstanding multi-functional properties, as well as the lead-free material. It belongs to the "rare" group of materials, multi-ferroics, showing simultaneous magnetic and ferroelectric properties, which are usually called the magneto-electric phenomenon, whereby this material has also many other useful features. Specifically, the first feature represents the high ferroelectric remnant polarization in the crystallographic direction (111) of 100 μC cm^{-2}, which goes far beyond the polarization of PZT. This is the largest known value of polarization among the perovskites, and that is why the ferrite is therefore interesting for application in the ferroelectric memory cell. In addition, $BiFeO_3$ has a high Curie temperature of about 825 °C (far above the room temperature), which designates this material among potentially interesting high temperature piezoelectric materials [2–5].

Based on previous literature data, the piezoelectric coefficient d_{33} for $BiFeO_3$ is in the range of 15–60 pm V^{-1} [6]. One of the strategies for increasing the piezoelectric response is to create a new solid melts based on the ferrite. Because of its rhombohedral crystal structure, $BiFeO_3$ has become interesting to the emergence of the morphotropic phase boundary (MPB). These boundaries separate the two phases, a passage between them, and the corresponding chemical composition. At such borders, dielectric, ferroelectric and piezoelectric properties are maximal.

In the current work, the detailed analysis of the product was performed by X-ray diffraction (XRD) powder analysis additionally supported by Rietveld refinement technique. Characterization of surfaces and microstructural profiles were performed using the scanning electron microscope (SEM) and transmission electron microscope (TEM). The magnetic properties of material were measured by vibrating-sample magnetometer (VSM) measurements. The spectroscopic analyses, which include the Fourier transform infrared spectroscopy (FTIR), the micro-Raman (MR) spectroscopy, and also the electron paramagnetic resonance (EPR) spectroscopy, were also applied. All these techniques have been applied to study characteristics of hydrothermally prepared $BiFeO_3$ powder in order to extract the critical information and give new insights in its structure on nanoscale.

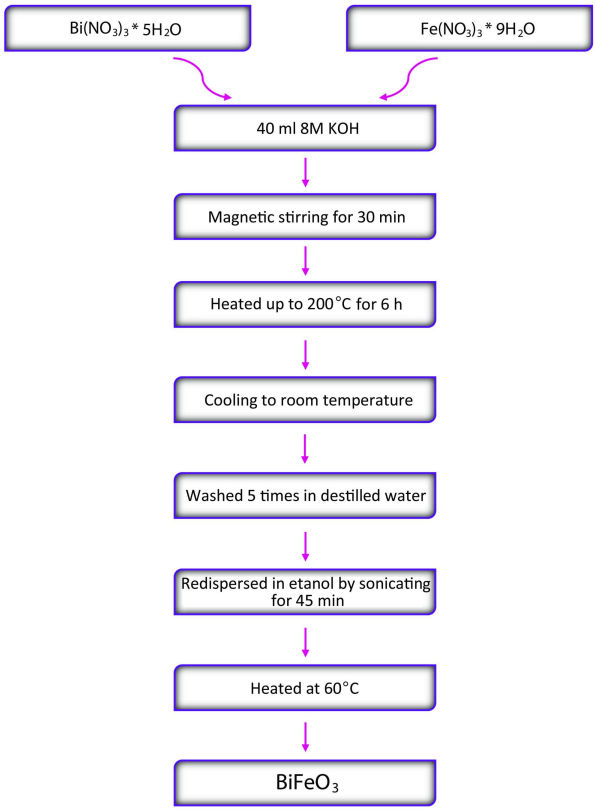

Figure 1. Flowing chart scheme for entire synthesis route of $BiFeO_3$ powders

In this work, we selected hydrothermal route in order to synthesize bismuth ferrite powders with small particle dimensions, high purity and crystallinity. In obtaining such characteristics of fine powders, we have focused on the most precise and fully controlled experimental procedure that would lead us to preparation of such products which would be useful in nanotechnology applications. This is very important issue because many of the useful properties of perovskite materials are critically dependent on the crystallite size.

II. Experimental

2.1. Synthesis of $BiFeO_3$ powders

The chemical regents used in this work were bismuth nitrate [$Bi(NO_3)_3 \cdot 5\,H_2O$], iron nitrate [$Fe(NO_3)_3 \cdot 9\,H_2O$] and potassium hydroxide (KOH). All the chemicals had analytical grade purity and were used as-received without further purification. In this paper, the procedure proposed by Han [7] was applied.

The equimolar mixtures of $Bi(NO_3)_3 \cdot 5\,H_2O$ and $Fe(NO_3)_3 \cdot 9\,H_2O$ were dissolved in 40 mL of KOH. The mixture was transferred into the autoclave where constant magnetic stirring for 30 min was applied. The autoclave was sealed, heated up to 200 °C and held for 6 hours, and then allowed to cool down to the room temperature.

The produced powders were collected at the bottom of the Teflonliner after cooling to the room temperature. The products were washed at least five times by the repeated cycles of centrifugation in distilled water, and re-dispersed in ethanol by sonication for 45 min. Subsequently, the powder was obtained by evaporating ethanol in a mortar heated at the temperature of T = 60 °C. The appropriate flowing chart scheme for entire synthesis route of $BiFeO_3$ powders is given in Fig. 1. In addition, the obtained powder was annealed at 800 °C for 2 h.

2.2. Characterization of synthetized powders

Characterization of crystalline material was performed by X-ray powder diffraction on a Rigaku UL-

TIMA IV XRPD diffractometer with Cu K$\alpha_{1,2}$ radiations, at the room temperature. The XRD data were recorded in a 2θ range of 20–80°, with the step of 0.02° and the scan speed of 2°/min. The complete analysis of the X-ray data was obtained using the Rietveld refinement.

The scanning electron microscopy (SEM) was employed for the characterization of particle morphology. The powder was sonicated in ethanol for 5 min; immediately afterwards, a drop of solution was cast onto a freshly cleaved "Kish" graphite (i.e. natural graphite ores; "Kish" graphite is produced by the fractional crystallization of carbon from molten steel) crystal embedded with a silver paste into a sample holder. Excess material was removed in a stream of argon gas. The sample was first annealed at 90 °C for 15 min in air, and afterwards degassed in low vacuum for 30 min. Characterization was performed at the room temperature by a Tescan MIRA3 (Tescan Orsay Holding, Brno, Czech Republic) field emission gun scanning electron microscope at 10 kV in a high vacuum.

Transmission electron microscopy (TEM) was used to determine the particle size and morphology. Analyses were performed on the transmission electron microscope TEM JEM-2100F (JEOL Ltd., Tokyo, Japan) operating at 200 kV, with field emission gun (FEG) electron source and equipped with Si(Li) energy-dispersive X-ray spectrometer (Link ISIS-300, Oxford Instruments, Oxfordshire, UK). In addition, the selected area electron diffraction (SAED) was performed in order to determine phase composition of the sample in the selected areas.

A vibrating-sample magnetometer (7397 Series Vibrating-sample magnetometer VSM, Lake Shore Cryotronics, Inc., USA) was used to investigate the magnetic properties of the sample at the room temperature in a magnetic field up to 15 kOe.

The FTIR spectrum was recorded in a transmission, on Thermo Fisher Scientific Nicolet™ iS™ 50 FT-IR (Thermo Fisher Scientific, USA) spectrometer. Tablets for measurement were prepared by mixing ~0.2 mg of the sample with 80 mg of KBr. Recording was conducted with 64 scenes and at a resolution of 2 cm^{-1}. After recording, the automatic baseline correction and atmospheric suppression (for elimination of emissions of CO_2 and H_2O) were done.

The micro-Raman spectra were collected in the backscattering configuration using TriVista 557 Raman (Princeton Instruments, USA) system. The 514.5 nm line of an Ar^+/Kr^+ mixed gas laser was used as an excitation source with an incident laser power less than 60 mW in order to minimize the heating effects.

The electron paramagnetic resonance (EPR) experiments were performed on X-band Magnettech MS300 (Magnettech GmbH, Germany) spectrometer operating at a nominal frequency of 9.5 GHz. The microwave power was 3.16 mW (the microwave attenuation of 15 dB), with a modulation amplitude of 0.1 mT. The Magnettech g-factor ZnS : Mn standard was used as the reference sample.

III. Results and discussion

3.1. XRD data analysis

Figure 2 shows the XRD pattern of the synthesized bismuth ferrite, $BiFeO_3$ (BFO) powder. The diffraction pattern was recorded at the room temperature and atmospheric pressure and in the absence of any re-heating of the sample. A fitting refinement procedure using the Rietveld method was performed. As shown in Fig. 2, the presented XRD pattern is dominated by diffraction peaks from bismuth ferrite. The external appearance of XRD pattern indicates that the final product is the single-phase and highly crystalline BFO. Consequently, diffraction peaks of the BFO powders synthesized with 8 M KOH can be indexed to a pure BFO phase. Figure 3 shows the XRD pattern of the BFO powders synthesized with 8 M KOH and annealed at 800 °C during 2 hours. The results of the Rietveld refinement for both considered systems are given in Table 1.

Bismuth ferrite crystallizes in the perovskite type structure (α-$BiFeO_3$) with rhombohedral space group *R3c* (No. 161) [8]. However, it may be seen in representation of cell parameters (Table 1) that hexagonal settings have been used. The Rietveld diagrams show

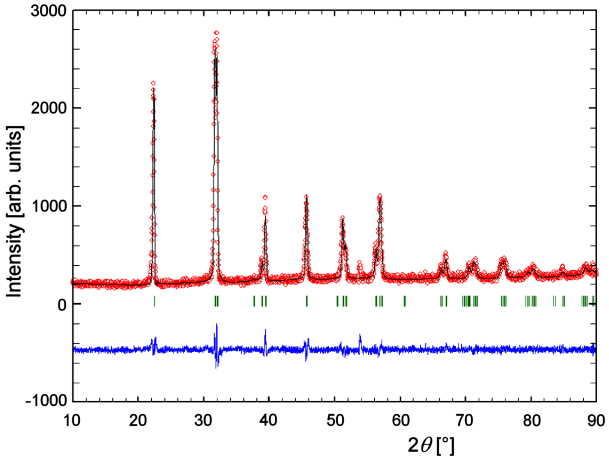

Figure 2. XRD pattern and Rietveld refinement of BFO powder synthesized with 8 M KOH for 6 h at 200 °C

Table 1. Rietveld refinement results for synthesized BFO and annealed (800 °C) samples

Sample	Synthesized BFO	Annealed BFO at 800 °C
Space group	*R3c*	*R3c*
a [Å]	5.5870(2)	5.5839(2)
b [Å]	5.5870(2)	5.5839(2)
c [Å]	13.8879(7)	13.8809(6)
α	90°	90°
β	90°	90°
γ	120°	120°
Crystallite size [nm]	43	52

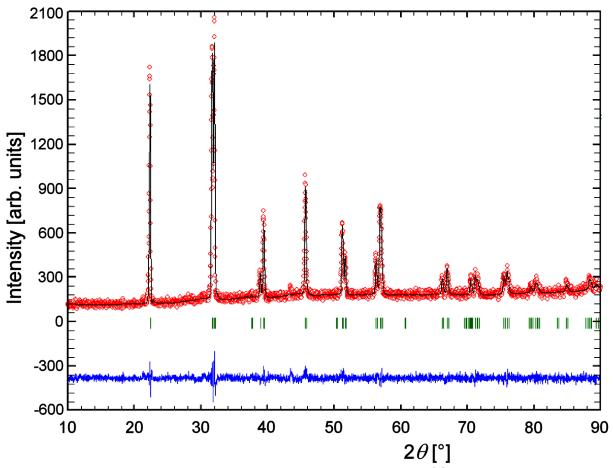

Figure 3. XRD pattern and Rietveld refinement of BFO powder annealed at 800 °C during 2 h

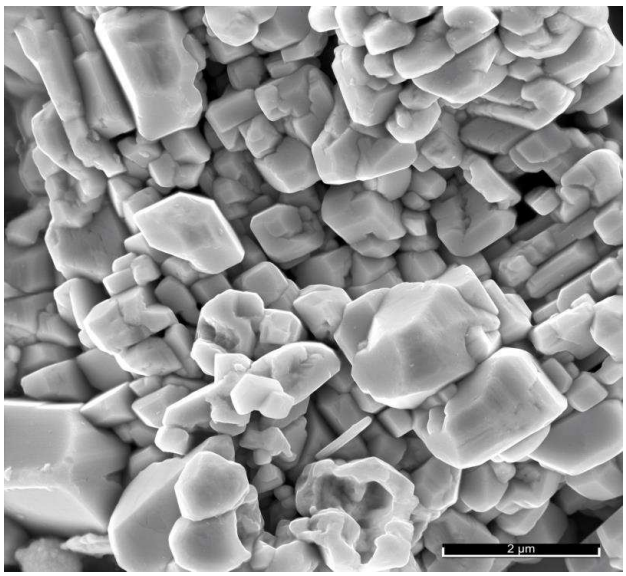

Figure 4. SEM image of BFO synthesized with 8 M KOH for 6 h at 200 °C (bar length is 2 μm)

good agreement between theoretical model and the experimental results. In the case of the synthesized BFO sample (Fig 2), another reflection of a secondary phase apparently can be seen at about 55.2°, while for the annealed sample at 800 °C (Fig 3) this reflection stands at approximately 45.2°. However, there is not enough data to identify the type of very small amount of this secondary phase. Besides the difference in unit cell parameters, the determined crystallite size in both samples showed that the crystallite size increases after annealing at 800°C.

3.2. SEM and TEM results

The effects of thermal treatment through applied hydrothermal method on morphology of the obtained BFO grains were evaluated by SEM analysis. The SEM image of the specimen synthesized by hydrothermal method at 200 °C for 6 hours is shown in Fig. 4. It can be seen that the resulting powder contains particles with a fairly regular polyhedron shapes, no pronounced "flattening" and the average particle size of approximately 300 nm. Our experimental procedure leads to the agglomerated powders. Also, in Fig. 4, we can observe the appearance of some regular cubic shape particles. The growth of large cubic grains (see for example the lower left corner of the SEM image in Fig. 4) is usually preferred for the hydrothermal approach [9]. Also, from Fig. 4 we can see that the elongated and circular particles do not exist and thus, it can be assumed that the energy transferred to the system is sufficient for the stage in which there is a normal growth of BFO phase. Therefore, in our considered case, the temperature as an important factor is monitored and maintained properly, without disturbing the equilibrium within the system.

The morphology of the obtained BFO particles was examined by TEM. The typical TEM images are shown in Fig. 5. In addition, SAED analyses over one of the grains were also conducted, which indicates the very sharp diffraction spots typical for the single crystals (inset in Fig. 5a). Based on the results reported in Fig. 5a,

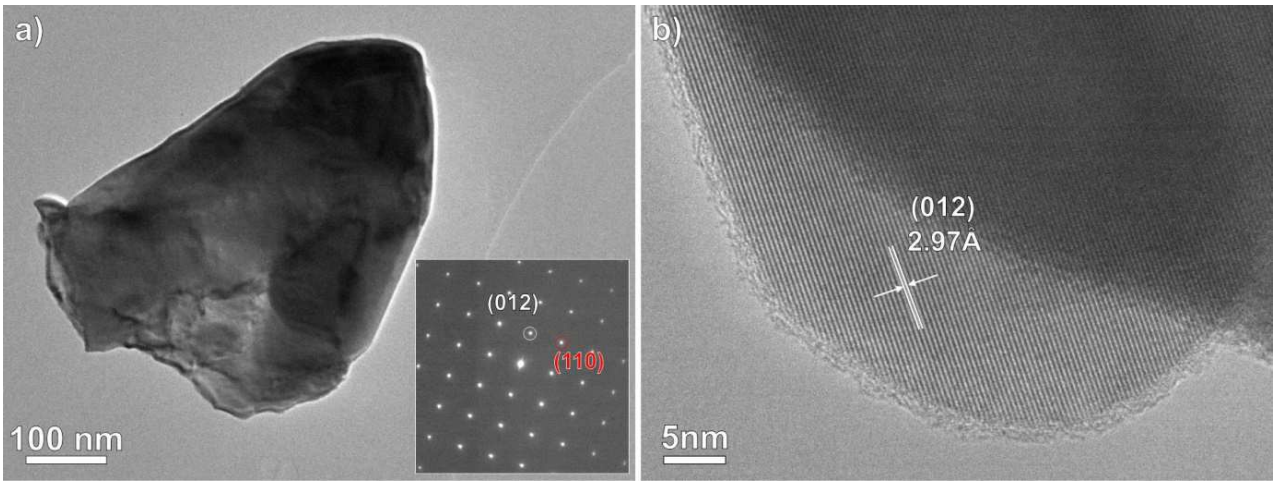

Figure 5. TEM image of a typical BFO particle (insert - SAED pattern over one grain) (a) and HRTEM image with characteristic *d*-spacing value (b)

it may be seen that the sample grains are very well crystallized, with obvious and clearly non-fragmented crystal flats. The index analysis clearly shows the existence of rhombohedral $BiFeO_3$ grains. Further analysis with the HRTEM (Fig. 5b) of individual particles confirms a clear evidence of the ultra-fine single crystal structure, showing an interplanar spacing of d = 2.97 Å, corresponding to (012) crystal planes. Consequently, the (012) d-spacing in $BiFeO_3$ plays an important role in A-site and/or B-site substitution, which represents the most effective way to reduce the impurity phases and enhance magneto-electric coupling constant by creating the lattice strain due to the ionic size mismatch between the host and substituting cations.

It should be noted that the diffraction spots of SAED pattern in this state are well-defined and in good agreement with the rhombohedral structure of the BFO particles with a lattice constant a (Table 1). These results are in fairly good agreement with the results of BFO nanoparticles synthesized by the wet chemical techniques [10,11]. HRTEM image demonstrates monocrystalline nature of the particle and the existence of twin stacking faults (Fig. 5b) in the synthesized powder. These identified crystallographic stacking faults can also enhance the magnetic properties of actual particles. It should also be noted that the stacking faults may be responsible for strain relaxation in fine particles, and thus influencing the magnetoelastic energy. Higher operating temperatures cause the grains to grow much bigger, so that we can obtain sharper monocrystal SAED image, as shown in Fig. 5a.

3.3. Vibrating-sample magnetometry measurements

In the next stage of the actual investigation, magnetization versus magnetic field (M-H) hysteresis loop was determined and the result was displayed in Fig. 6. Evaluated loop at the room temperature within the applied field of 15 kOe reveals that the particles show typical ferromagnetic character. The observed loop exhibits a finite exchange bias field and vertical asymmetry with visible magnetization saturations. This behaviour could be a result of the uniform particle sizes and additional lattice strains caused by the large amount of surface atoms from the small grain size.

The M-H hysteresis loop of the synthesized particles exhibit a single-phase-like magnetization behaviour and does not show the linear curve feature typical for bulk material. From the qualitative point of view this indicates that a large portion of the specimen was converted into the particles from bulk powder. Magnetization should be expected to have an almost linear behaviour with external magnetic field at elevated operating temperature (above 600 °C) which would mean that specimen lost its ferromagnetic property. This phenomenon may be expected for larger crystallites (>62 nm) [12] and display the bulk lattice parameters, where in this case the hysteresis loop will be lost. This situation is not identified in our study.

It was found [13,14] that doping with magnetically active Tb^{3+} ions having radius smaller than that of Bi^{3+} ion results in a larger distortion in the lattice structure thereby leading to the suppression of the spiral spin modulation in $BiFeO_3$. This is precisely because the spin cycloid of Tb^{3+}, which got destroyed in the structural transformation of rhombohedral to orthorhombic structure. It should be mentioned that the BFO nanoparticles with other sizes could be modeled by a superposition of an antiferromagnetic core and a ferromagnetic surface. As a result, the ferromagnetism contributed by the uncompensated spin surface increases as the particle size decreases.

3.4. FTIR results

Figure 7 shows the FTIR spectrum of the $BiFeO_3$ powder derived from the hydrothermal reaction, which is synthesized at the operating temperature of 200 °C. The peaks at positions of 440 and 539 cm^{-1} can be attributed to the modes of Fe–O stretching vibrations and Fe–O bending vibration, respectively. This behaviour is characteristic of [FeO_6] octahedra in the perovskites

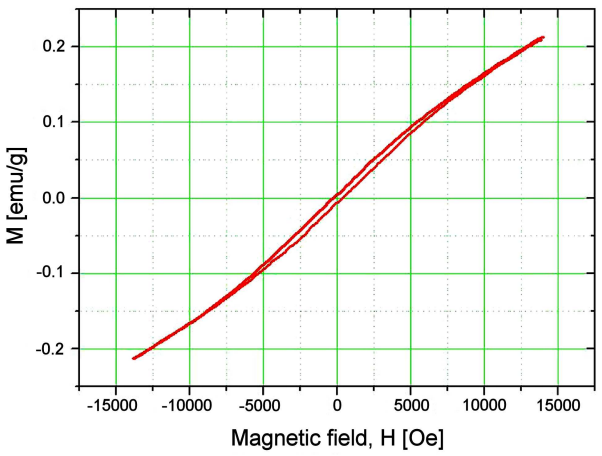

Figure 6. VSM measurement of BFO powder, at room temperature in a maximum magnetic field of 15 kOe

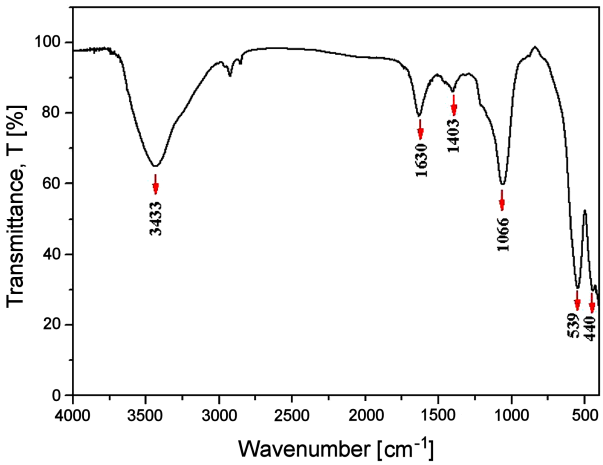

Figure 7. FTIR spectrum of BFO powder synthesized with 8 M KOH for 6 h at 200 °C

[15]. The band at around 1066 cm^{-1} can be attributed to the vibration of Bi–O bond [16]. The broad band in the region of 3000–3600 cm^{-1} is the result of antisymmetric and symmetric stretching of H_2O and OH^- bond groups, while band at 1630 cm^{-1} corresponds to the bending vibrations of H_2O [17]. The band at 1403 cm^{-1} was due to the presence of trapped nitrates [18]. The residual water and hydroxyl groups are usually detected in the as-synthesized samples and further heat treatment is necessary for their elimination. It is well known that the hydroxylation of metal ions and deprotonation can be accelerated by raising the solution temperature or pressure [19].

3.5. Raman spectroscopy

In the Raman spectrum (Fig. 8), the positions of the Raman peaks were fitted by using a Lorentzian profile and the positions of each Raman mode are given in the top right corner of the image. The Raman mode positions are in good agreement with reported literature data [20]. The peak at 138.16 cm^{-1} can be assigned to the first normal A_1 mode for the rhombohedral $BiFeO_3$ system. Calculations suggested that the most dominant force constant for other A_1 modes in $BiFeO_3$ system can be ascribed to Bi–O1, suggesting the relatively more important contribution of Bi–O bonds to the observation of the optical phonon modes as compared with that of Fe–O bonds. The decrease in the peak intensity of this normal A_1 mode (Fig. 8) may be an indication of suppression of contribution of Bi–O1 vibrational mode, which most likely can be attributed to enhanced coupling of magnetic, ferroelectric and structural order parameters due to size confinement considerations and accompanying lattice distortions in the prepared $BiFeO_3$. Decrease in intensity of the peak positioned at 138.16 cm^{-1} coincides with appearance of an appreciable spontaneous magnetization and hysteretic behaviour.

Bearing in mind the two characteristic peaks (at 138.16 cm^{-1} (peak A_a) and 168.44 cm^{-1} (peak B_b)) related to A_1 modes, the ratio of integral intensities of a given peaks can be determined. It has been found that the reducing trend in I_{A_a}/I_{B_b} may be observed for the BFO particles smaller than 62 nm, which coincides very well with its enhanced ferromagnetic properties. The BFO powder (<62 nm) shows a sizeable hysteresis and finite coercivity due to the breaking of helical ordering or the incomplete rotation of the spins along the antiferromagnetic axis which give rise to the higher magnetization. From Fig. 8, we can notice the existence of strongest peak situated at 74.28 cm^{-1} (E – mode) which confirms the FE (ferroelectric) nature of BFO and can be associated with the motion of Bi–O bonds (it may be the most sensitive to the magnetic transitions and likewise the transitions of dielectric origin), which controls the dielectric constant [21]. It is known both theoretically and experimentally that the FE ordering in BFO is governed by the stereochemically active Bi^{3+} ions with $6s^2$ lone pair, which takes part in the relatively lower wavenumber Raman modes in BFO (<168 cm^{-1}). Raman peak at 74.28 cm^{-1} represents one of the most intense peaks, and it can be expected that this peak possess ability of shifting behaviour with the temperature change. Thus, this anomaly could indicate the coupling of FE and the spin excitations associated with magnetic cycloid for a particle sizes less than 62 nm [22].

All of the 13 Raman-active phonon modes in the Raman spectra may exhibit slight differences in the peak positions depending on the size of particles, and may be due to the changes in the oxygen bonding and disorder [23,24].

3.6. EPR result

The EPR spectra of the BFO powder at 77 and 293 K are presented in Fig. 9. The intensity of EPR line is higher, and the line is sharper at the room temperature. The intensity of EPR line at the room temperature does not saturate with power, contrary to the EPR line at LN temperature which saturates. The behaviour at the LN temperature is due to the freezing of spins. Decrease

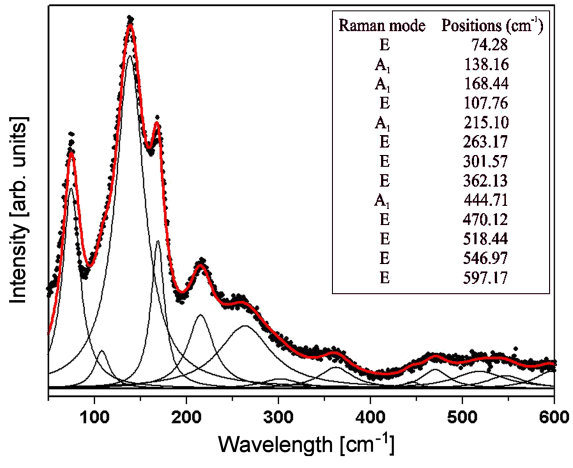

Figure 8. Experimentally obtained Raman spectrum of BFO powder prepared by hydrothermal method (dots) and fitted spectrum (line) using the Lorentzian type profile (positions of each Raman mode are given in inset)

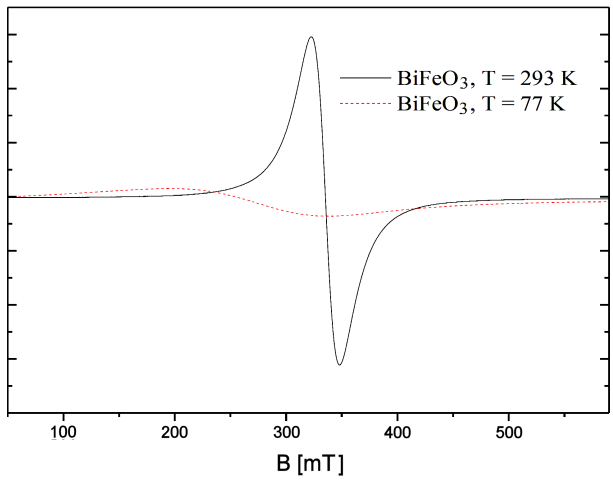

Figure 9. EPR spectra of the BFO powder measured at T = 293 K and T = 77 K

of the intensity and resonant field and increase of linewidth with decrease of temperature is a sign of superparamagnetic behaviour. The resonant field is lower (g-value is higher) at the LN temperature due to increased internal field. The change of g factor from the free electron value, $\Delta g = 0.47$, is proportional to expression $(D/J) \cdot g$, where D is the magnitude of Dzyaloshinskii-Moriya vector and J is the super-exchange constant.

The EPR line at the room temperature is strong, with $g = 2.0195 \pm 0.0005$, peak-to-peak line-width $\Delta H_{PP} = 26 \pm 0.5$ mT and can be well described with a single Lorentzian line. Such line is attributable to the Fe^{3+} ions in an octahedral environment. This result can be ascribed to Fe ions and can be correlated with the resonant absorption in the cycloidal spin structure and defect induced free spins. Striking absorption splits were not observed (Fig. 9), where there is no change in magnetic environment for the unpaired electrons in Fe ions, and also absence of the iron exchange-coupled magnetic secondary phase. It is evident that there is no any sign of EPR line at $g \sim 4$ (where the theoretical g factor was expressed in terms of the spin Hamiltonian) which is characteristic of Fe^{3+} ions in a low symmetry environment (the tetragonal coordinated Fe^{3+} ions) (characteristic of magnetically isolated high spin Fe^{3+} ($s = 5/2$)), which corresponds to defect complex, e.g. $(Fe^{2+}_{Fe^{3+}} - V^{\bullet\bullet}_{O})^{\bullet}$ the defect dipoles. The transition from the room temperature down to LN temperature and change in the intensity of the EPR line can arise from the spin-reorientation and stems out of the charge localization at the low temperature and thermally-activated hopping-induced ferromagnetic interactions. Moreover, the degree of canting of spins is also related with the g-value and the large g-value results in a severe spin canting. A possible explanation of the observed EPR spectrum involves the electrons trapped by vacancies or defects, which is suggested by the fact that obtained g-value is slightly larger than 2 (2.0195). It should also be noted that existence of $Fe^{3+}-O_V$ defect complex may be generated at elevated temperatures as it follows the formation of trivalent iron ions, which provide local 3d moments. These local magnetic moments may be involved in ferromagnetic behaviours. Our results show that is a sure way to stabilize the perovskite state and to induce the ferromagnetism at the room temperature in $BiFeO_3$ is in fact a 3d element doping procedure within the materials engineering research.

Metallic ions may distribute randomly over the octahedral sites of the face-centred cubic unit cell as an ideal symmetry. On the heating disordered manners, the oxygen ion arrangement remains unchanged but the cations order themselves over the octahedral sites, resulting in a larger unit cell of a lower symmetry (tetragonal). The paraelectric phase of $BiFeO_3$ does not take the cubic perovskite-like structure which arises from the energy difference between the prototypical cubic structure and the equilibrium ferroelectric *R3c* structure which amounts 1.1 eV/f.u. [25]. In fact, the several low symmetric atomic arrangements based on tetragonal and rhombohedral structures are found at the lower total energy than cubic perovskite-type structure.

IV. Conclusions

Detailed characterization of $BiFeO_3$ (BFO) powders synthesized by the strictly controlled hydrothermal process was conducted. X-ray analysis of non-annealed powder showed that BFO can be perfectly fitted to a rhombohedral space group *R3c*, where external appearance of XRD patterns indicate that the final product is a single-phase material with high crystallinity. Besides difference in the unit cell parameters for the sample annealed 800 °C, it was shown that there is an increase in the crystallite size. SEM analyses showed that grains are very well crystallized, with non-fragmented crystal flats. Further analysis with the HRTEM of individual particles confirmed the evidence of ultra-fine single crystal particles, with characteristic (012) crystal planes. Furthermore, HRTEM confirmed the existence of twin stacking faults, which are responsible for enhanced magnetic properties of synthesized fine particles. The Raman spectroscopy analysis showed the enhanced coupling of the magnetic, ferroelectric and structural order parameters due to the size confinement considerations and accompanying the lattice distortions in the prepared BFO particles. The EPR results suggested the existence and participation of electrons trapped by vacancies or defects. It has been proposed that the existence of $Fe^{3+}-O_V$ defect complex could be generated at elevated temperatures followed by formation of trivalent Fe ions, which intensely provide the local 3d moments.

Acknowledgement: This research work was partially supported by the Serbian Ministry of Education, Science and Technological Development under the projects No. 172015, 172018 and III 45012. We are also grateful to Jelena Zagorac ("Vinča" Institute of Nuclear Sciences, Serbia) for Rietveld refinement calculations and Nadežda Stanković ("Vinča" Institute of Nuclear Sciences, Serbia) for performed TEM analyses with the helpful comments, and also Aleksandar Matković and Bojan Stojadinović (Institute of Physics, University of Belgrade, Serbia) for SEM and Raman spectroscopy measurement evaluations.

References

1. J. Rödel, W. Jo, K.T.P. Seifert, E.-M. Anton, T. Granzow, D. Damjanovic, "Perspective on the development of lead-free piezoceramics", *J. Am. Ceram. Soc.*, **92** (6) (2009) 1153–1177.
2. V. Fruth, L. Mitoseriu, D. Berger, A. Ianculescu, C. Matei, S. Preda, M. Zaharescu, "Preparation and characterization of $BiFeO_3$ ceramic", *Progress Solid State Chem.*, **35** (2007) 193–202.
3. M.S. Bernardo, "Synthesis, microstructure and prop-

erties of $BiFeO_3$-based multiferroic materials: A review", *Bol. Soc. Esp. Ceram. Vidr.*, **53** (2014) 1–14.
4. K. Liu, H. Fan, P. Ren, C. Yang,"Structural, electronic and optical properties of $BiFeO_3$ studied by first-principles", *J. Alloys Comp.*, **509** (2011) 1901–1095.
5. M. Popa, D. Crespo, J.M. Calderon-Moreno, "Sythesis and structural characterization of single-phase $BiFeO_3$ powders from a polymeric precursor", *J. Am. Ceram. Soc.*, **90** (9) (2007) 2723–2727.
6. G. Catalan, J.F. Scott, "Physics and applications of bismuth ferrite", *Adv. Mater.*, **21** (2009) 2463–2485.
7. S.H. Han, K.S. Kim, H.G. Kim, H.-G. Lee, H.-W. Kang, J.S. Kim, C.I. Cheon, "Synthesis and characterization of multiferroic $BiFeO_3$ powders fabricated by hydrothermal method", *Ceram. Int.*, **36** (2010) 1365–1372.
8. D.C. Arnold, "Composition-driven structural phase transitions in rare-earth-doped $BiFeO_3$ ceramics: A review", *IEEE Trans. Ultrason. Ferroelec. Freq. Control*, **62** (2015) 62–82.
9. R. Haumont, I.A. Kornev, S. Lisenkov, L. Bellaiche, J. Kreisel, B. Dkhil, "Phase stability and structural temperature dependence in powdered multiferroic $BiFeO_3$", *Phys. Rev. B*, **78** (2008) 134108.
10. V.I. Zinenko, M.S. Pavlovskii, "Lattice dynamics of $BiFeO_3$: The untypical behavior of the ferroelectric instability under hydrostatic pressure", *JETP Lett.*, **87** (2008) 288–291.
11. S. Komarneni, V.C. Menon, Q.H. Li, R. Roy, F. Ainger, "Microwave-hydrothermal processing of $BiFeO_3$ and $CsAl_2PO_6$", *J. Am. Ceram. Soc.*, **79** (1996) 1409–1412.
12. E. Shi, C.T. Xia, W.Z. Zhong, B.G. Wang, C.D. Feng, "Crystallographic properties of hydrothermal barium titanate crystallites", *J. Am. Ceram. Soc.*, **80** (1997) 1567–1572.
13. A.Z. Simões, E.C. Aguiar, A.H.M. Gonzalez, J. Andrés, E. Longo, J.A. Varela, "Strain behavior of lanthanum modified $BiFeO_3$ thin films prepared via soft chemical method", *J. Appl. Phys.*, **104** (2008) 104115.
14. S. Kumar, "Structural, dielectric and magnetic characterization of Gd doped $BiFeO_3$ nanopowders", *Mater. Focus*, **2** (2013) 48–52.
15. C. Chen, J. Cheng, S. Yu, L. Che, Z. Meng, "Hydrothermal synthesis of perovskite bismuth ferrite crystallites", *J. Cryst. Growth*, **291** (2006) 135–139.
16. I.O. Troyanchuk, A.N. Chobot, O.S. Mantytskaya, N.V. Tereshko, "Magnetic properties of $Bi(Fe_{1-x}M_x)O_3$ (M = Mn, Ti)", *Inorg. Mater.*, **46** (2010) 424–428.
17. G.S. Lotey, N.K. Verma, "Multiferroic properties of Tb-doped $BiFeO_3$ nanowires", *J. Nanopart. Res.*, **15** (2013) 1553–1566.
18. T.-J. Park, G.C. Papaefthymiou, A.J. Viescas, A.R. Moodenbaugh, S.S. Wong, "Size-dependent magnetic properties of single-crystalline multiferroic $BiFeO_3$ nanoparticles", *Nano Lett.*, **7** (2007) 766–772.
19. G.S. Lotey, N.K. Verma, "Magnetodielectric properties of rare earth metal-doped $BiFeO_3$ nanoparticles", *J. Mater. Sci. Mater. Electr.*, **24** (2013) 3723–3729.
20. R.C. Lennox, M.C. Price, W. Jamieson, M. Jura, A. Daoud-Aladine, C.A. Murray, C. Tang, D.C. Arnold, "Strain driven structural phase transformations in dysprosium doped $BiFeO_3$ ceramics", *J. Mater. Chem. C*, **2** (2014) 3345–3360.
21. Y. Hu, L. Fei, Y. Zhang, J. Yuan, Y. Wang, H.Gu, "Synthesis of bismuth ferrite nanoparticles via a wet chemical route at low temperature", *J. Nanopart.*, **2011** (2011) 1–6.
22. K. Nakamoto, *Infrared and Raman Spectra of Inorganic and Coordination Compounds*, John Wiley & Sons, New York, USA, 1997, pp. 70–75.
23. A.V. Zalesskii, A.A. Frolov, T.A. Khimich, A.A. Bush, "Composition-induced transition of spin-modulated structure into a uniform antiferromagnetic state in a $Bi_{1-x}La_xFeO_3$ system studied using 57Fe NMR", *Phys. Solid State*, **45** (2003) 134–138.
24. H. Wang, J.J. Zhu, J.M. Zhu, X.H. Liao, S. Xu, T. Ding, H.Y. Chen "Preparation of nanocrystalline ceria particles by sonochemical and microwave assisted heating methods", *Phys. Chem. Chem. Phys.*, **4** (2002) 3794–3799.
25. D. Kothari, V.R. Reddy, V.G. Sathe, A. Gupta, A. Banerjee, A.M. Awasthi, "Raman scattering study of polycrystalline magneto-electric $BiFeO_3$", *J. Magn. Mag. Mater.*, **320** (2008) 548–552.